Proceedings Paper:
Xu, H, Zacur, E, Schneider, JE et al. (1 more author) (2019) Ventricle Surface Reconstruction from Cardiac MR Slices Using Deep Learning. In: Coudière, Y, Ozenne, V, Vigmond, E and Zemzemi, N, (eds.) Lecture Notes in Computer Science. FIMH 2019: Functional Imaging and Modeling of the Heart, 06-08 Jun 2019, Bordeaux, France. Springer Verlag , pp. 342-351. ISBN 9783030219482

https://doi.org/10.1007/978-3-030-21949-9_37

Ventricle surface reconstruction from CMR slices using deep learning

First Author[1][0000−1111−2222−3333], Second Author[2,3][1111−2222−3333−4444], and Third Author[3][2222−−3333−4444−5555]

1 **********
2 **********
3 **********

Abstract. Reconstructing 3D ventricular surfaces from 2D cardiac MR data is challenging due to the sparsity of the input data and the presence of interslice misalignment. It is usually formulated as a 3D mesh adaption problem often incorporating shape priors and smoothness regularization, which might affect accuracy when handling pathological cases. We propose to formulate the 3D reconstruction as a volumetric mapping problem followed by isosurfacing from dense volumetric data. Taking advantage of deep learning algorithms, which learns to predict each voxel lable without explicitly defining the shapes, our method is capable of generating anatomically meaningful surfaces with great flexibility. The sparse 3D volumetric input can process contours with any orientations and thus can utilize information from multiple short- and long-axis views. In addition, our method can provide correction of motion artefacts. We have validated our method using a statistical shape model on both reconstructing 3D shapes from spatially consistent and misaligned input data.

Keywords: Mesh reconstruction · Cardiac MRI · Deep learning.

1 Introduction

Generating anatomically accurate 3D surface meshes has shown promising uses in a wide range of applications including cardiac function analysis, interventional guidance and diagnosis [1, 2, 3]. Personalization of cardiac surfaces in 3D is also the first step required for computational simulations of cardiac electromechanics using the finite element method [4, 5, 6]. Cardiac MR (CMR) imaging provides accurate shape information of the heart non-invasively [2]. A standard clinical CMR study includes a stack of short-axis (SAX) slices, covering at least from the left/right ventricular (LV/RV) apex to the base, plus at least two long-axis (LAX) views: horizontal long-axis (HLA, also known as 4 chamber view or 4CH) and vertical long-axis (VLA, also known as 2 chamber view or 2CH) [7]. Classical isosurfacing algorithms cannot be directly used due to the sparsity of the input data and because of the presence of motion artefacts (misalignment between slices caused by multiple breath holding and possible body movement during

acquisition) [8], which make the task of reconstructing 3D structure from CMR data particularly challenging.

Reconstruction of 3D surfaces from CMR data is normally formulated as a 3D mesh adaptation problem to sparse contours or points [9, 10, 11, 12], and solutions often incorporate shape priors during that process. The form of such prior could be a regular shape [10, 11, 13] or a statistical template with plausible variations [14], and deviations from regular and smooth geometries are penalized in a fitting process. These methods usually include an explicit smoothing term during fitting to further regularize the shape in addition to the use of shape priors, and both types of bias may compromise the accuracy of the reconstructed surfaces when handling pathological hearts. [15, 16]. In order to generate anatomically meaningful surfaces while also preserving the wide variability of the shape, reconstruction methods should incorporate a wide collection of plausible shape priors to refer to when fitting the input data. Deep learning algorithms have shown their capacity for storing a large number of accurate mappings between pair-wised data [17], and no explicit smoothing term is required by these methods, allowing the appearance of sharp edges and corners during reconstruction if necessary. However, for Convolutional Neural Networks (CNNs), input data are required to be highly structured (usually on a regular grid in 2D or 3D), and therefore most state-of-the-art deep learning methods for generating LV and RV 3D meshes using CMR data only take the SAX stack as input with the assumption that all SAX images are in parallel.[18, 19] This implementation limits the possibility of utilizing the LAX slices, which has been shown to improve the reconstruction of the ventricular meshes [12], as well as the possibility of incorporating out-of-plane geometric transformations for better correction of motion artefacts due to respiration [20, 21].

In this paper, we propose to consider the sparse 3D information from contours in a volumetric form, and therefore tackle the problem similarly to volumetric image inpainting [22]. We then transform the problem of mesh fitting from sparse input into a 3D volumetric mapping problem followed by isosurfacing from dense volumetric data. The sparse volumetric input can take contours in any positions within the volume, and therefore our method incorporates both SAX slices and LAX slices, and allows explicit out-of-plane motion artefact correction. Our method also has the capacity of reconstructing 3D meshes from misaligned input contours by itself.

1.1 Main Contributions

We have developed a novel bi-ventricular mesh reconstruction method through 3D volumetric mapping with deep learning algorithm combining both SAX and LAX slices. To our best knowledge, this is the first deep learning method processing multiple views simultaneously without any assumption of image plane orientations.

We propose the method that can be used to reconstruct 3D meshes from both spatially consistent and misaligned input data, and our method is capable

of processing intersecting slices with discrepancies among them, while most of the state-of-the-art methods still focusing on parallel contours.

2 Materials and Methods

Our 3D reconstruction method consisted of three steps: 1. generating sparse volumetric input data from contours; 2. generating dense 3D volumetric predictions of LV myocardium and LV/RV cavities from input data using a variation of the 3D U-Net [23]; 3. generating 3D meshes from the predictions with an isosurfacing algorithm. The method is developed and evaluated by using synthetic data generated from a statistical shape model [14, 24].

2.1 Data

We used the statistical shape model published by Bai et al [14], in which the authors registered 1093 segmented hearts to a template space using rigid registration followed by the application of principal component analysis (PCA) to the surface meshes. The model is formed by labeled images with labels for background, LV myocardium and LV/RV cavities. We downloaded from the publicly available dataset (http://wp.doc.ic.ac.uk/wbai/data/), the mean shape model, the first 100 PCs and the corresponding eigenvalues or variances. We then used these to generate 120 different shapes. limiting the variations to six standard deviations for any of the PCs.

To generate output references, we placed these shapes into a 3D volume with the size of $128 \times 128 \times 128$ and voxel size of $2 \times 2 \times 2$ mm^3, by aligning the centre of the smallest sphere enclosing the corresponding contours and the centre of the 3D volume, and labled voxels enclosed by surfaces accordingly. To simulate input sparse volumes in conditions similar to real clinical acquisition, we used real image planes from clinical datasets (consisting of both SAX stack and two LAX slices). To generate spatially consistent input datasets, we first aligned one set of image planes to each of the shapes, and the voxels located within 0.5 mm away from the planes were then given their original labels. Voxels located more than 0.5 mm away from the plane is asigned to label of Unknow. To mimic the misalignment caused by motion artefacts, we first fixed image planes and before assigning labels for each plane we applied random rotations with no larger than 10 degrees and random translations with no more than 4 mm to the reference shape. An example of input and output volumetric data is shown in Figure 2.

2.2 Volumetric Mapping

We adapted a variation of 3D U-Net for volumetric mapping, and the schematic diagram of the network architecture is shown in Figure 1. The network consists of an encoder and a decoder, with skip connections between feature maps with the same resolution. The encoder starts from the input layer with the size of $128 \times 128 \times 128 \times 1$ and has three max-pooling stages where each pooling layer

has a window size of (2, 2, 2) and a stride of (2, 2, 2), giving feature maps with four different resolutions. The decoder then up-samples the feature maps back to the original resolution also in three stages using upsampling layers with factors of (2, 2, 2). The heavy duty of the computation within the network is carried out by convolutional blocks shown in Figure 1, with each of them having two convolutional layers with kernel size of (3, 3, 3) and two batch normalisation (BN) layers. Other than the output layer, which has sigmoid activation functions, rectified linear units (ReLU) are used throughout the network. The output layer has 3 convolutional kernels with the size of (1, 1, 1) giving the prediction in the form of $128 \times 128 \times 128 \times 3$ volume representing LV myocardium, LV cavity and RV cavity. The Dice coefficient loss was used during the training of the network to deal with imbalance between forground and background voxels. [25]

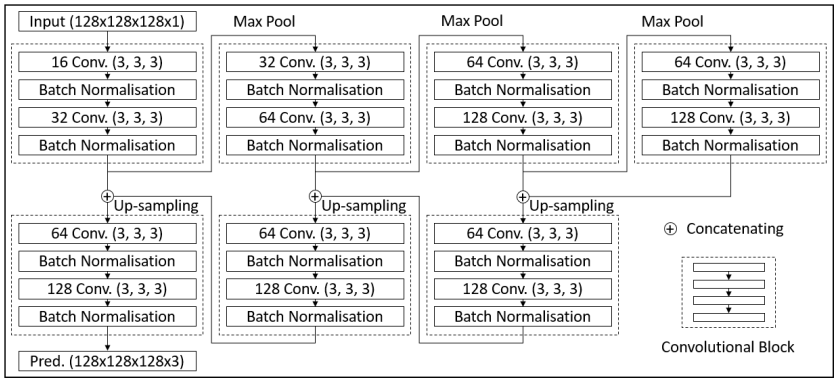

Fig. 1. A schematic diagram of our volumetric mapping network. For each convolutional layer, the number of filters is specified respectively.

2.3 Isosurfacing

The prediction of the network was split into three of $128 \times 128 \times 128$ volumes, and used to form the isosurfaces at 0.5 using marching cubes [26]. For each 3D volume, the largest object was then selected as the expected structure.

3 Experiments and Results

We performed two 4-fold cross-validation experiments with spatially consistent data and misaligned data respectively. For both experiments, the same number of bi-ventricular shapes were generated as described in section 2.1, and they were randomly grouped into 4 sets of training data (80 shapes), validating data (10 shapes) and testing data (30 shapes) also in the same way, having 4 testing

datasets cover all generated shapes. During the training phase of each cross-validation experiment, one neural network was randomly initiated and the network parameters were updated through back-propagation using the spatially consistent training data. The optimization was early stopped by evaluating the loss function of the validating data to prevent over-fitting. Once the training of the neural network for the spatially consistent cases was terminated, the learned parameters were used to initiate the network for reconstructing misaligned cases and fine-tuned using the misaligned training data. An overview of the training progress is shown in Figure 2. The testing data was only used for the evaluation of the method, and the predictions from the network for the testing data were then used to generate 3D meshes as described in section 2.3. In both experiments Dice coefficient and Hausdroff Distance (HD) were the metrics used for quantitative analysis of the method. For the experiment with misaligned contours we registered the reconstructed shape to the reference shape with a rigid transformation before calculating the metrics. We also calculated Euler characteristic for the generated meshes to evaluate the topology of them, and for all cases the value was expected to be equal to 2.

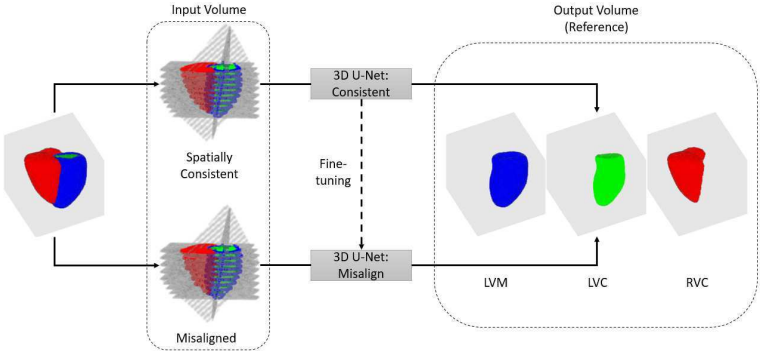

Fig. 2. Training progress overview. The blue, green, red objects correspond to LV myocardium, LV cavity and RV cavity.

3.1 Statistical Shape Model

The Dice coefficient and HD results for experiments on spatially consistent and misaligned contours are shown in Table 1. For spatially consistent input data, the reconstructed LV/RV cavities shape and the reference shape has Dice coefficient with mean values of 0.98. The LV myocardium has a more complicated shape with larger surface area, and therefore the Dice score is more sensitive with small changes, while the mean value is still 0.94. The voxel size is $2 \times 2 \times 2\ mm^3$, and the mean values of HD are around 2 voxels. As the input data has only around 5.5% of voxels with known labels, the results suggest that our 3D U-Net stored

a collection of plausible mappings between sparse input data and corresponding ventricular shapes during training and is able to utilize that information during the reconstruction of the testing cases.

Table 1. Dice coefficient and Hausdorff Distance between reconstructed ventricular shape and reference ventricular shape for both spatially consistent and misaligned slices experiments. The Dice coefficient has values between 0 and 1 and Hausdorff Distance is in mm. The metrics are presented in the form of mean ± standard deviation.

	Consistent			Misaligned		
	LVM	LVC	RVC	LVM	LVC	RVC
Dice	0.94 ± 0.01	0.98 ± 0.01	0.98 ± 0.01	0.83 ± 0.04	0.95 ± 0.01	0.93 ± 0.02
HD (mm)	4.56 ± 1.66	3.17 ± 1.07	3.87 ± 2.28	6.30 ± 5.21	4.94 ± 3.61	5.91 ± 2.55

The experiments on misaligned input data also achieved good accuracy, with above 0.93 mean Dice coefficient for LV/RV cavities and 0.83 for LV myocardium. As expected, comparing to the experiment on spatially consistent input data, the accuracy of these experiment is lower. This is unavoidable given the additional challenges involved in reconstructing the 3D shapes from misaligned input data, including discrepancies between slices, which results in the same set of input data maps to a much wider range of plausible output shapes.

It is important to highlight the limitations of the validation method itself. The misalignment of all slices, combined, will result in an overall rigid transformation of the underlying three-dimensional shape. This rigidly transformed shape if the most likely to be reconstructed by our network. If we compare this reconstruction with the original shape, the accuracy will be significantly affected, even if the shapes are exactly equal. We attempted at compensating for this unwanted effect by performing a rigid registration, but this still leaves residual errors that are partly responsible for the decrease of accuracy shown in Table 1.

For more than 85% of the 3D meshes directly generated from network predictions, the Euler characteristic is 2, suggesting a robust network output with no isolated false predictions, holes within the object or handles attached to it. However, post-processing described in section 2.3 is still needed and increases the rate by 8%.

3.2 Real Contours

We also applied our method on real contours, and one example of reconstructed meshes aligned with input contours were shown in Figure 3. Our method reconstructed one set of plausible 3D meshes for LV myocardium and LV/RV cavities. The structure has no obvious distortions caused by misalignment, and the reconstructed meshes align well with the input contours.

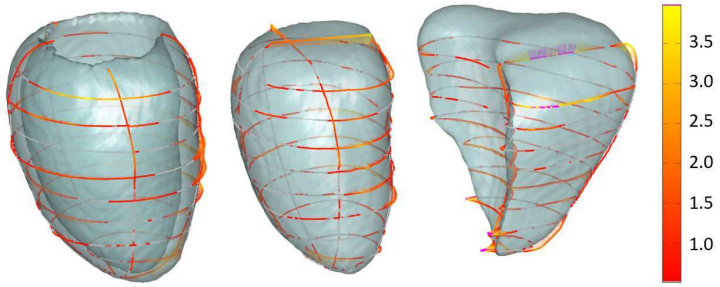

Fig. 3. Real contours aligned with reconstructed meshes. The colours indicate the closest distance from the contours to meshes. For distance smaller than 0.5 *mm* the colour is gray, and for distance larger than 4 *mm* the colour is purple. Colours corresponding to distance between 0.5 *mm* and 4 *mm* are shown in the colour bar.

4 Conclusions

In this paper, we propose a bi-ventricular 3D mesh reconstruction method from CMR slices by transforming the mesh fitting problem into a volumetric mapping problem followed by isosurfacing. Our method takes the advantage of deep learning algorithm and is able to reconstruct anatomically meaningful surfaces with a wide range of variety for both spatially consistent and misaligned contours. The method has no constrains on the slice orientations and utilizes information from multiple SAX and LAX views simultaneously. It tolerates discrepancies between intersecting slices, and produces accurate 3D meshes from misaligned cases. We developed and evaluated our method using cases generated from a statistical shape model. We also applied our method to real contours and achieved good quality reconstructed meshes.

References

1. Vukicevic, M.; Mosadegh, B.; Min, J.; Little, S. Cardiac 3D Printing and its Future Directions. JACC Cardiovasc. Imaging 2017, 10, 171184.
2. Suinesiaputra A., Ablin P., Alba X., Alessandrini M., Allen J., Bai W., Cimen S. et al. "Statistical shape modeling of the left ventricle: myocardial infarct classification challenge." IEEE JBHI 22, no. 2 (2018): 503-515.
3. Lehmann, H.; et al. Integrating Viability Information into a Cardiac Model for Interventional Guidance. In Proceedings of the 5th FIMH, 35 June 2009; pp. 312320.
4. Zacur E., et al. "MRI-based heart and torso personalization for computer modeling and simulation of cardiac electrophysiology." In Proceedings of BIVPCS 2017 and POCUS 2017, pp. 61-70. Springer, Cham, 2017.
5. Arevalo, H., et al. Arrhythmia risk stratification of patients after myocardial infarction using personalized heart models. Nat. Commun. 2016, 7, 11437.
6. Deng, D.; Zhang, J.; Xia, L. Three-Dimensional Mesh Generation for Human Heart Model. Life Syst. Model. Intell. Comput. 2010, 98, 157162.

7. AHA Writing Group on Myocardial Segmentation and Registration for Cardiac Imaging:, Manuel D. Cerqueira, et al. "Standardized myocardial segmentation and nomenclature for tomographic imaging of the heart: a statement for healthcare professionals from the Cardiac Imaging Committee of the Council on Clinical Cardiology of the American Heart Association." Circulation 105, no. 4 (2002): 539-542.
8. Villard B., Zacur E., DallArmellina E., and Grau V.. Correction of slice misalignment in multi-breath-hold cardiac MRI scans. STACOM 2016.
9. Zou, M.; Holloway, M.; Carr, N.; Ju, T. Topology-Constrained Surface Reconstruction From Cross-sections. ACM Trans. Graph. 2015, 34, 128.
10. Young, A.; et al. Left Ventricular Mass and Volume: Fast Calculation with Guide-Point Modelling on MR Images. Radiology 2000, 2, 597602.
11. Medrano-Gracia P., Cowan B. R., Bluemke D. A., Finn J. P., Lima J. AC, Suinesiaputra A. , and Young A. A.. "Large scale left ventricular shape atlas using automated model fitting to contours." In IMFH, pp. 433-441. 2013.
12. Villard B., Grau V., and Zacur E.. "Surface Mesh Reconstruction from Cardiac MRI Contours." Journal of Imaging 4, no. 1 (2018): 16.
13. Lamata, P.; et al. An accurate, fast and robust method to generate patient-specific cubic Hermite meshes. Med. Image Anal. 2011, 15, 801813.
14. De Marvao, A.; et al. Population-based studies of myocardial hypertrophy: High resolution cardiovascular magnetic resonance atlases improve statistical power. J. Cardiovasc. Magn. Reson. 2015, 16, 16.
15. Zhang X., Cowan B. R., Bluemke D. A., Finn J. P., Fonseca C. G., Kadish A. H., Lee D. C. et al. "Atlas-based quantification of cardiac remodeling due to myocardial infarction."PloS one9, no. 10 (2014): e110243.
16. Alba X., Pereanez M., Hoogendoorn C., Swift A. J., Wild J. M., Frangi A. F., and Lekadir K.. An algorithm for the segmentation of highly abnormal hearts using a generic statistical shape model. IEEE TMI, 35(3):845859, 2016.
17. Zhang C., et al. "Understanding deep learning requires rethinking generalization." arXiv preprint arXiv:1611.03530 (2016).
18. Oktay O., Ferrante E., Kamnitsas K., Heinrich M., Bai W., Caballero J., Cook S. A. et al. "Anatomically constrained neural networks (ACNNs): application to cardiac image enhancement and segmentation." IEEE TMI 37, no. 2 (2018): 384-395.
19. Duan J., et al. "Automatic 3D bi-ventricular segmentation of cardiac images by a shape-refined multi-task deep learning approach." IEEE TMI (2019).
20. McLeish, K.; Hill, D.L.G.; Atkinson, D.; Blackall, J.M.; Razavi, R. A study of the motion and deformation of the heart due to respiration. IEEE TMI 2002.
21. Shechter, G.; Ozturk, C.; Resar, J.R.; McVeigh, E.R. Respiratory motion of the heart from free breathing coronary angiograms. IEEE TMI 2004, 23, 10461056.
22. Bertalmio M., Sapiro G., Caselles V., and Ballester C.. "Image inpainting." In-Proceedings of the 27th annual conference on Computer graphics and interactive techniques, pp. 417-424. ACM Press/Addison-Wesley Publishing Co., 2000.
23. Cicek O., et al. "3D U-Net: learning dense volumetric segmentation from sparse annotation." In MICCAI, pp. 424-432. 2016.
24. Bai, W.; Shi, W.; de Marvao, A.; Dawes, T.; ORegan, D.; Cook, S.; Rueckert, D. A bi-ventricular cardiac atlas built from 1000+ high resolution MR images of healthy subjects and an analysis of shape and motion. Med. Image Anal. 2015, 26, 133145.
25. Milletari, F., Navab, N. and Ahmadi, S.A.. V-net: Fully convolutional neural networks for volumetric medical image segmentation. In 4th 3DV (pp. 565-571). 2016
26. Lorensen, William E., and Harvey E. Cline. "Marching cubes: A high resolution 3D surface construction algorithm." In ACM siggraph computer graphics, vol. 21, no. 4, pp. 163-169. ACM, 1987.